

RE-ASSESSMENT OF CANONICAL AND NON-CANONICAL ADVERSE-PRESSURE-GRADIENT TURBULENT BOUNDARY LAYERS

Ramis Örlü*, Ricardo Vinuesa, Philipp Schlatter

Linné FLOW Centre, KTH Mechanics, Stockholm, Sweden

*ramis@mech.kth.se

Carlos Sanmiguel Vila, Stefano Discetti, Andrea Ianiro

Aerospace Engineering Group, University Carlos III of Madrid, Leganés, Spain

Abstract. The present paper first summarises the concerted experimental and numerical efforts initiated at KTH on zero-pressure gradient turbulent boundary layers. Starting from an assessment of available numerical data sets of this canonical flow, existing discrepancies are discussed and their origin is related to different inflow and tripping histories. Criteria are then established to discern development effects from genuine features of this flow case. The second part is devoted to the effect of an adverse pressure gradients on turbulent boundary layers. In particular, a number of direct and large-eddy simulations covering a wide range of pressure-gradient parameters and streamwise histories on flat and curved surfaces is performed and is compared with wind-tunnel experiments utilising hot-wire anemometry and particle image velocimetry that overlap and extend the Reynolds number range of the in-house numerical simulations. The effect of different pressure-gradient histories is exemplified on mean and turbulence quantities and a first attempt to separate Reynolds-number and pressure-gradient effects on turbulent boundary layers is presented.

Keywords: Wall Turbulence, Turbulent Boundary Layer, Pressure-Gradient Effects

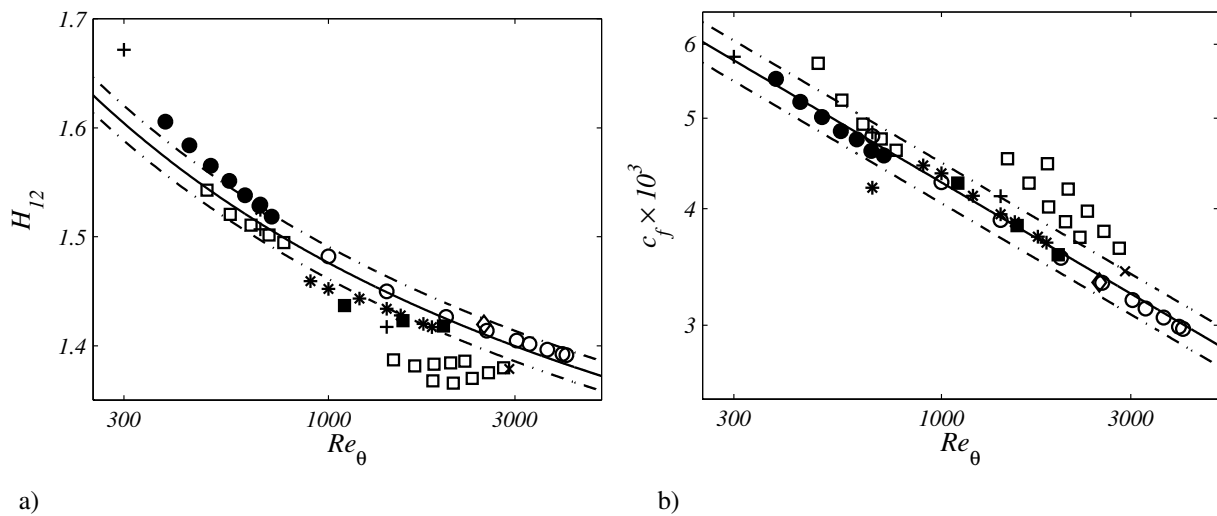
1. BACKGROUND: LESSONS FROM ZPG TURBULENT BOUNDARY LAYER STUDIES

Starting with the work by Schlatter *et al.* (2009) a fruitful collaboration between experimental and simulation efforts at KTH Mechanics was initiated with respect to spatially-developing zero-pressure-gradient (ZPG) turbulent boundary layers. This work provided, for the first time, a concerted effort to cross-validate wind-tunnel experiments and direct numerical simulations (DNS) of turbulent boundary layers at the same computationally high and experimentally low momentum-thickness based Reynolds number Re_θ of 2500. The agreement in terms of skin-friction coefficient, mean velocity, and turbulent fluctuations, was excellent and the results allowed for a substantial reduction of the uncertainty in boundary-layer data, and cross-validated the numerical setup and experimental technique.

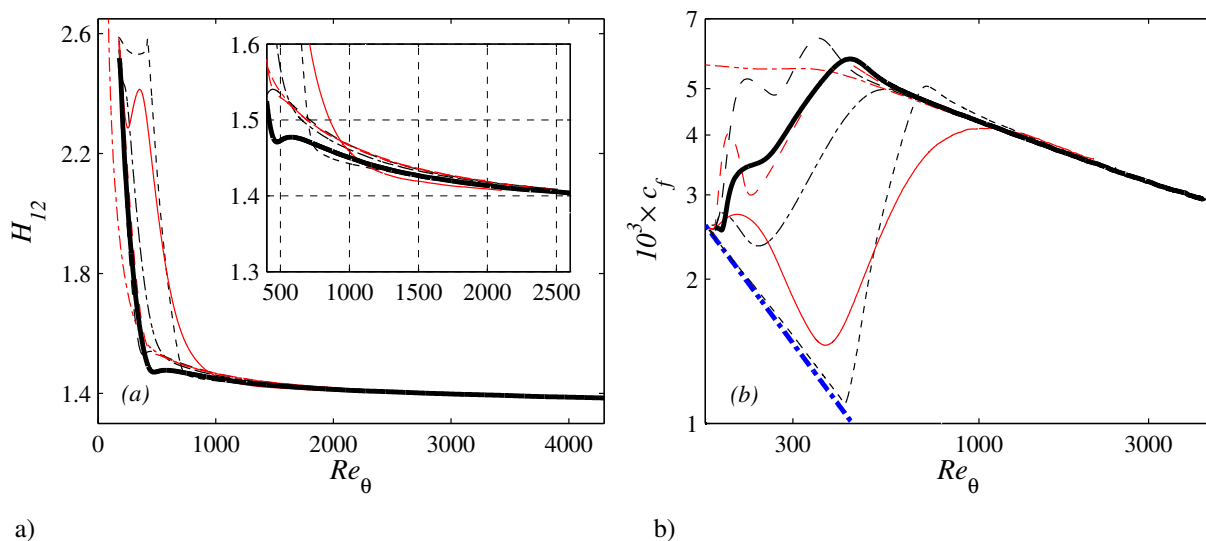
Based on this success, these efforts were then extended to $Re_\theta = 4300$ by means of large-eddy simulations (LES) (Schlatter *et al.*, 2010) upon which a DNS on a finer grid was performed reaching the same Re (Schlatter and Örlü, 2010a). The resolution of this DNS is comparable to high- Re channel-flow simulations such as e.g. Hoyas and Jiménez (2006) and slightly higher than in the previous boundary-layer simulation (Schlatter *et al.*, 2009). The same publication also presented a unique compilation of existing DNS data sets pertaining to canonical turbulent boundary layers under zero-pressure-gradient (ZPG) conditions. Such an assessment has previously only been performed (or considered necessary) for experimental data sets (see e.g. Fernholz and Finley, 1996; Chauhan *et al.*, 2009). Although all of these simulations relate to the same physical flow case, the approaches differed in terms of the numerical method, grid resolution and distribution, inflow-generation method, boundary conditions and box dimensions. The resulting comparison for these high-quality simulations showed surprisingly large differences not only in both basic integral quantities such as the shape factor or skin-friction coefficient as depicted in figure 1, but also in their predictions of mean and fluctuation profiles far into the sublayer (where differences were not expected). It could thus be shown that the numerical simulation of turbulent boundary layers is, mainly due to the spatial development of the flow, very sensitive to, e.g. proper inflow condition, sufficient settling length and appropriate box dimensions. The conclusion of this investigation was that a DNS has to be considered as a numerical experiment and should be the subject of the same scrutiny as experimental data.

In order to illuminate the reason for the unexpectedly large differences between various DNS data sets as apparent from figure 2, the effect of inflow and tripping effects in spatially-developing zero-pressure-gradient turbulent boundary layer flows was systematically investigated by means of DNS (Schlatter and Örlü, 2012). These simulations showed that different inflow conditions and tripping effects could indeed explain most of the differences observed when comparing available DNS at low Re . It could further be shown that, if transition was initiated at a low enough Reynolds number $Re_\theta < 300$, all quantities would agree well for both the inner and outer layer for $Re_\theta > 2000$. This result gave thereby a lower limit for meaningful comparisons between numerical and/or wind-tunnel experiments, assuming that the flow was not severely over- or understimulated (e.g. through the tripping).

Based on these results, a detailed comparison between the aforementioned DNS and experiment of a turbulent boundary layer under ZPG conditions at moderate Reynolds numbers was performed (Örlü and Schlatter, 2013). Integral and



a) b)
 Figure 1. *a)* Shape factor, $H_{12} = \delta^*/\theta$, as function of Reynolds number. The solid line represents integration of the composite profile by Chauhan *et al.* (2009) including an ad-hoc low- Re correction (cf. equation (8) in Chauhan *et al.*, 2009), while the dash-dotted lines indicate a 1% tolerance. *b)* Skin-friction coefficient, c_f , as function of Reynolds number. Solid line represents the correlation by Smits *et al.* (1983) and dash-dotted lines indicate a 5% tolerance. Reprinted from Schlatter and Örlü (2012), to which the reader is referred for details. *Reproduced with permission from Cambridge University Press.*



a) b)
 Figure 2. *a)* Shape factor, H_{12} , and *b)* skin-friction coefficient, c_f , as function of Reynolds number, Re_θ , for various tripping conditions. Reprinted from Örlü and Schlatter (2013), to which the reader is referred for details (besides Schlatter and Örlü, 2012). *Reproduced with permission from Springer.*

global quantities have been found to agree very well and confirm quantitatively the correlations by Monkewitz *et al.* (2008) for the shape factor and skin-friction coefficient. Mean and fluctuating streamwise velocity profiles, including higher-order moments, and the probability density distribution have been found to agree remarkably well throughout the boundary layer. Differences within the buffer region for the higher-order moments could solely be related and traced back to insufficient spatial resolution effects of the employed hot-wire sensor (Örlü and Alfredsson, 2010), thereby highlighting the statistical identity of both the experimental and numerical data sets. Similarly, structural quantities, like the large-scale transport of small-scale energy related to the amplitude modulation of the small scales by means of large-scale fluctuations (Schlatter and Örlü, 2010b), have been shown to be alike to a high degree. The established identity of both data sets persists as well for the power spectral density.

The aforementioned efforts have also been extended to highly resolved large-eddy simulations for a spatially-developing turbulent boundary layer, covering in a single domain the range $Re_\theta = 180$ to 8300 (Eitel-Amor *et al.*, 2014). Turbulence statistics and integral values are in close agreement with experiments and other simulations. This and the aforementioned DNS data sets have e.g. been used to tackle the question of whether distinct hairpin vortices are significant or even present

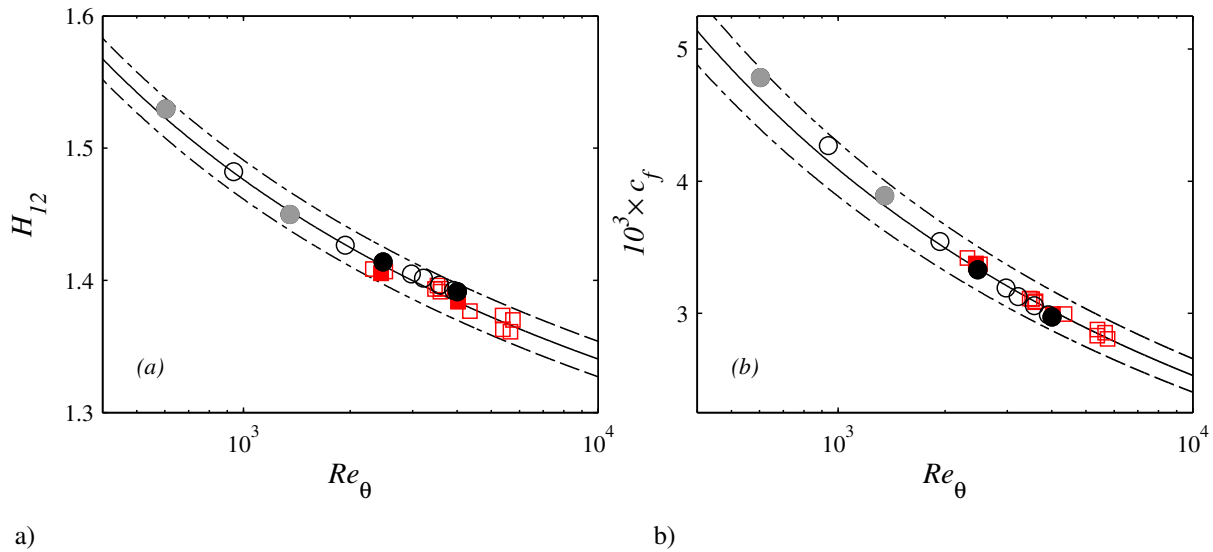


Figure 3. (a) Shape factor, H_{12} , as function of Reynolds number Re_θ . The solid line represents integration of the composite profile by Chauhan *et al.* (2009) including an ad-hoc low- Re correction (*cf.* equation (8) in Chauhan *et al.* (2009)), while the dash-dotted lines indicate a 1% tolerance. (b) Skin-friction coefficient, c_f , as function of Reynolds number. The solid line represents the Coles-Fernholz skin friction relation with $\kappa = 0.384$ and $C = 4.127$ (Nagib *et al.*, 2007) and the dash-dotted lines indicate a 5% tolerance. Numerical and experimental data are indicated through \circ and \square , respectively. Reprinted from Örlü and Schlatter (2013), to which the reader is referred for details. *Reproduced with permission from Springer.*

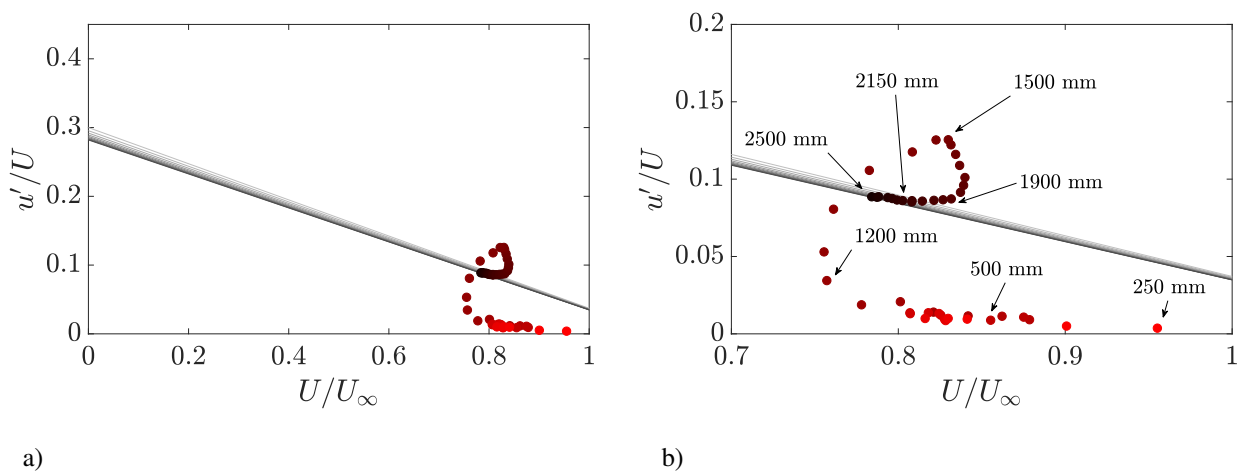


Figure 4. a) Diagnostic-plot methodology as a design tool demonstrated using the ZPG TBL with a non-optimal (i.e. weak and late) tripping configuration. Solid lines correspond to the diagnostic plot slope with $Re_\theta = 1,000$ (light grey) to 10,000 (dark grey) (10 logarithmically-spaced cases). b) Zoom-in of a) with indicated streamwise locations of the measurement points taken with equidistant streamwise spacings of $\Delta x = 50$ mm. Reprinted from Sanmiguel Vila *et al.* (2017b), to which the reader is referred for details. *Reproduced with permission from Cambridge University Press.*

close to the wall. Results based on these data sets clearly suggest that in turbulent boundary layers, hairpin vortices may exist at low Reynolds numbers, induced by laminar-turbulent transition. However, they do not persist in great number in the fully developed region. Their dominant appearance as instantaneous coherent structures in the outer boundary-layer region is very unlikely (Schlatter *et al.*, 2014; Eitel-Amor *et al.*, 2015).

Connected to the numerical study in Schlatter and Örlü (2012), an experimental counterpart was performed in the Minimum Turbulence Level (MTL) wind tunnel at KTH, in order to define practically-realizable criteria to establish a well-behaved turbulent boundary layer. For that reason the diagnostic plot (Alfredsson and Örlü, 2010; Alfredsson *et al.*, 2011) was exploited, since it has the advantage that it only relies on measurements of the streamwise mean velocity and turbulence intensity at arbitrary wall-normal distances, and therefore uncertainties from the friction velocity u_τ or the

wall-normal distance y , among others, are eliminated with its use. Previous studies had shown that the outer region of turbulent boundary layers is universal in this scaling (Alfredsson *et al.*, 2012; Örlü *et al.*, 2016), namely, the turbulence intensity is linearly related to the mean velocity ratio. Since neither the skin-friction coefficient, shape factor or wake parameter, nor full velocity profile measurements are required, the idea to assess the streamwise development with a scan through the outer part of the turbulent boundary layer arose. More specifically, a hot-wire probe could, for instance, be placed within the outer part of the boundary layer and traversed downstream, thereby revealing the streamwise location from where on the turbulent boundary layer can be considered genuine and well-behaved. Figure 4 shows the results from a streamwise traverse while keeping (through an iterative procedure) a hot-wire probe within the velocity range $0.7 < U/U_\infty < 0.9$ through the outer part of a ZPG turbulent boundary layer. As apparent from the color-coded measurement points, indicating the streamwise distance from the leading edge (from lighter to darker symbols with increasing streamwise distance), the boundary layer is first laminar and then undergoes transition to turbulence with the associated overshoot in turbulence intensity.

2. FROM ZPG TO APG TURBULENT BOUNDARY LAYERS

Despite the importance of ZPG turbulent boundary layers from the viewpoint of fundamental research, most flows of relevance in technical applications are exposed to various pressure-gradients and to the effect of surface curvature, which instead may lead to changes of the form drag. The applicability of knowledge from canonical wall-bounded flows as outlined in the previous section is hence limited when it comes to these complex flows and geometries (see e.g. Patel and Sotiropoulos, 1997). Although a number of simulations (see e.g. Lee and Sung, 2008) and experiments (see e.g. Monty *et al.*, 2011) on adverse-pressure-gradient (APG) turbulent boundary layers, spanning a wide range of Reynolds numbers and values of the Clauser pressure-gradient parameter $\beta = \delta^*/\tau_w dP_e/dx$ (where δ^* is the displacement thickness, τ_w the mean wall-shear stress and dP_e/dx is the streamwise pressure gradient) have been performed in the past, it is hard to draw firm conclusions from the available data. One of the reasons explaining the difficulties in comparing the various datasets is the differently varying streamwise distributions of β , i.e. the various upstream histories leading to a particular pressure-gradient condition. The importance of inflow and tripping effects has become apparent from the aforementioned ZPG studies (Schlatter and Örlü, 2012; Sanmiguel Vila *et al.*, 2017b), and it is therefore anticipated that development effects are more complex and more crucial for turbulent boundary layers under APG conditions. The present contribution aims therefore at establishing different upstream histories on APG turbulent boundary layers both through simulations and experiments. For this purpose it was crucial to obtain APG turbulent boundary layers in which a region of constant β was observed over a sufficient downstream distance, in order to study the genuine effect of the imposed pressure gradient and its upstream history separately.

Since the effect of the pressure gradient on the turbulent boundary layers is closely related to its streamwise develop-

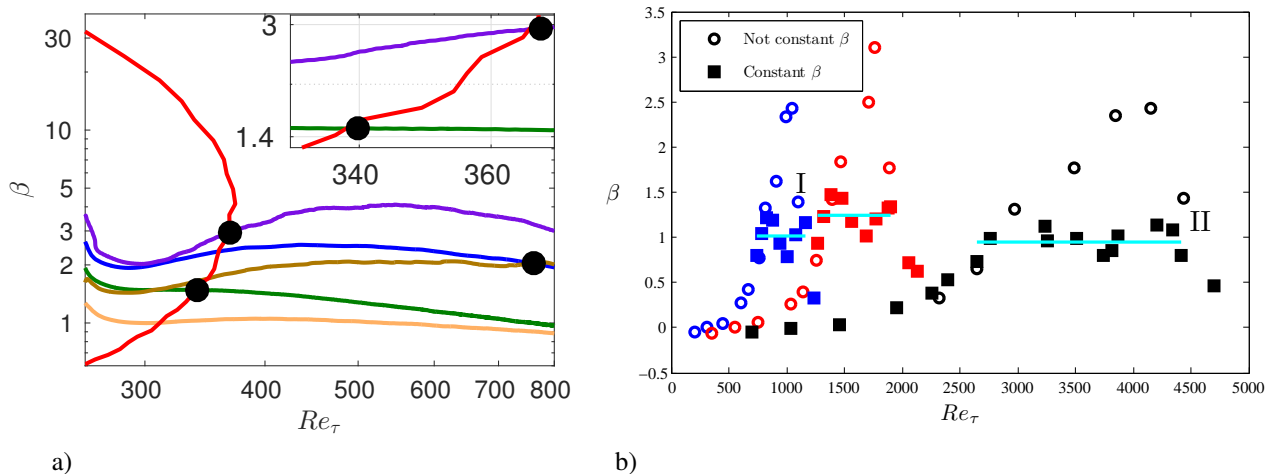


Figure 5. Clauser pressure-gradient parameter β as function of friction Reynolds number Re_τ . a) Simulations: — boundary layer developing on the suction side of a wing (Hosseini *et al.*, 2016), and over a flat plate for non-constant β -cases (— $m = -0.13$, — $m = -0.16$ and — $m = -0.18$) (Bobke *et al.*, 2016) and constant β -cases (— $\beta = 1$ and — $\beta = 2$) (Bobke *et al.*, 2017). Reprinted from Bobke *et al.* (2017), to which the reader is referred for details. *Reproduced with permission from Cambridge University Press.* b) Wind-tunnel experiments: Experiments were performed with inflow velocities of (blue) 6, (red) 12 and (black) 30 m/s. Comparisons between cases with different β histories are done at (I) $\beta \approx 1.2$, $Re_\tau \approx 1100$ and (II) $\beta \approx 1.2$ and $Re_\tau \approx 4500$. Cyan lines indicate the constant- β regions.

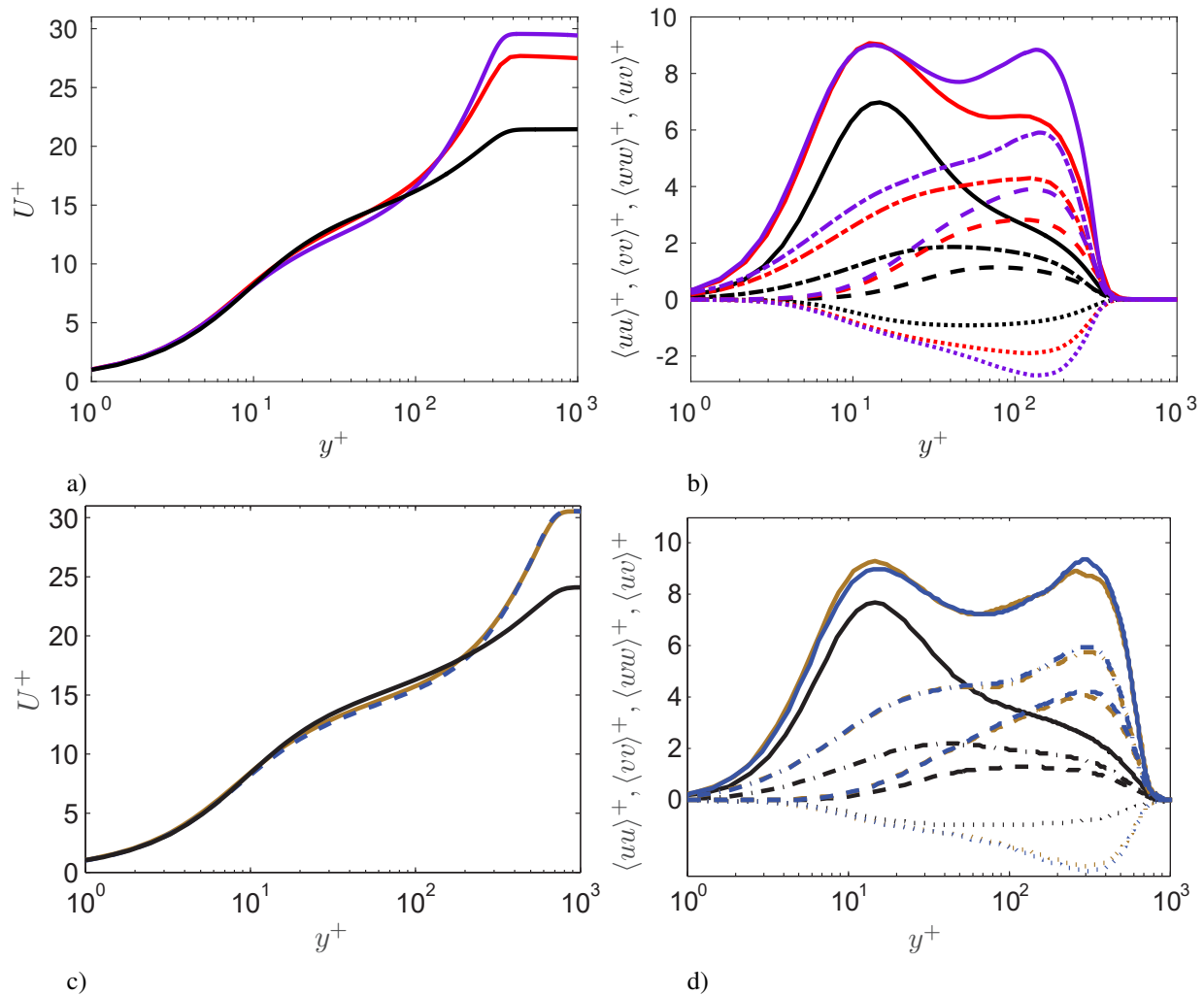


Figure 6. (a), (c) Inner-scaled mean velocity profiles and (b), (d) selected components of the inner-scaled Reynolds-stress tensor. (a), (b) correspond to $\beta = 2.9$ and $Re_\tau = 367$; and (c), (d) to $\beta = 2.0$ and $Re_\tau = 762$. For colours see caption of Figure 5a). Note that the black line corresponds to a ZPG TBL at matched Re_τ (Schlatter and Örlü, 2010a). Reprinted from Bobke *et al.* (2017), to which the reader is referred for details. *Reproduced with permission from Cambridge University Press.*

ment, it is important to define the concept of an equilibrium boundary layer: according to the strict definition by Townsend (1976), this condition requires the mean flow and Reynolds-stress tensor profiles to be independent of the streamwise position x , when scaled with appropriate local velocity and length scales. As also shown by Townsend (1976) this condition is only satisfied by the sink flow, although it is possible to define a less restrictive *near-equilibrium* condition when the mean velocity defect $U_\infty - U$ is self-similar in the outer region, which in any case dominates at high Reynolds numbers (Marusic *et al.*, 2010). Townsend (1976) and Mellor and Gibson (1966) showed that these near-equilibrium conditions can be obtained when the freestream velocity is prescribed by a power law such that $U_\infty = C(x - x_0)^m$, where C is a constant, x_0 is a virtual origin and m the power-law exponent. In particular, Townsend (1976) showed that m has to be larger than $-1/3$ in order to obtain near-equilibrium conditions, which means that all accelerated turbulent boundary layers subjected to a favourable pressure gradient (FPG), with U_∞ distributions defined by a power law, exhibit near-equilibrium behaviour. Regarding turbulent boundary layers subjected to APGs, only the ones with U_∞ defined by a power law as discussed above, and satisfying $-1/3 < m < 0$, are in near-equilibrium conditions. Further discussion on equilibrium in APG TBLs can be found in the work by Maciel *et al.* (2006).

For the present study, use is being made of a number of in-house direct numerical and large-eddy simulations in flat-plate ZPG (Schlatter and Örlü, 2010a, 2012) and APG turbulent boundary layers with both non-constant β (Bobke *et al.*, 2016) and constant β (Bobke *et al.*, 2017), as well as in APGs developing on wing sections (Hosseini *et al.*, 2016). The reader is referred to the respective papers for the specific parameters and simulation details. Additionally, an extensive experimental campaign was carried out at the MTL wind tunnel at KTH Royal Institute of Technology by means of hot-wire anemometry (HWA) and particle image velocimetry (PIV). The desired pressure-gradient conditions

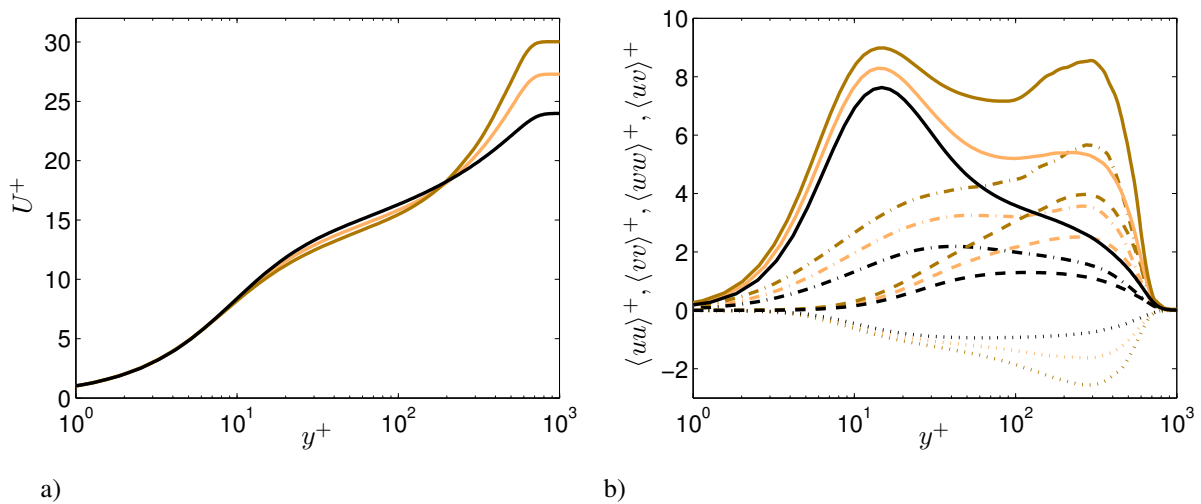


Figure 7. (a) Inner-scaled mean velocity profiles and (b) selected components of the inner-scaled Reynolds-stress tensor. Cases with constant values of $\beta = 0, 1$ and 2 , at matched friction Reynolds number $Re_\tau \simeq 700$. For colours see caption of Figure 5a), and note that the black line corresponds to a ZPG turbulent boundary layer at matched Re_τ (Schlatter and Örlü, 2010a). Reprinted from Bobke *et al.* (2017), to which the reader is referred for details. *Reproduced with permission from Cambridge University Press.*

and flow histories were established by means of wall inserts, and the wall-shear stress was measured by using oil-film interferometry (OFI) (Vinuesa and Örlü, 2017). The established pressure gradient and Reynolds number space is displayed in form of $\beta - Re_\tau$ plots as depicted in Figure 5 (note that Re_τ is the friction Reynolds number, formed with the friction velocity u_τ and the 99% boundary-layer thickness δ_{99}), which will later on be utilised to study the impact of particular β distributions on the state of the TBL by considering matching β and Re_τ values. Note that the determination of the boundary-layer thickness and edge velocity can become ambiguous and cumbersome the stronger the pressure gradient becomes, hence these quantities were determined by means of the method developed by Vinuesa *et al.* (2016).

The streamwise development of the five near-equilibrium APG turbulent boundary layers on flat plates obtained in the simulations (Figure 5a)), defined by different power-law exponents and virtual origins, is clearly distinguishable from the trend of the APG turbulent boundary layer on the suction side of a wing when considering the $\beta - Re_\tau$ plot. While β decreases over the streamwise direction in the cases denoted with m ($m13, m16, m18$), β remains constant for the two cases denoted with b ($b1, b2$). Regarding the cases with constant β , not only are they in near-equilibrium, but they also allow a better characterisation of Reynolds-number effects in a certain pressure-gradient configuration. Note that the ZPG turbulent boundary layer flow essentially corresponds to a constant $\beta = 0$ configuration. To further extend the Reynolds-number range, six of the experimentally realised β distributions are shown in Figure 5b). The effect of the different histories can be assessed when the cases under consideration have the same Reynolds number and APG magnitude, but have been subjected to different accumulated pressure-gradient effects due to the particular β distributions. Such matching conditions have been highlighted in figure 5 and will be discussed in terms of mean and turbulence quantities in the following.

In Figure 6 we show the inner-scaled mean streamwise velocity component for the various comparisons discussed above, as well as selected components of the Reynolds-stress tensor. The first two important observations from this figure are: although the two comparisons are at the same β and Re_τ , the turbulence statistics in the outer layer are essentially different among the cases, while they agree in the viscous sublayer. This highlights the significant impact of history effects on the state of the outer layer of a turbulent boundary layer. Focusing on Figure 6(a,c), we can observe the general effect of a moderate APG on the boundary layers, compared with the equivalent ZPG case: the APG turbulent boundary layers exhibit a steeper logarithmic region, as previously observed by Nagib and Chauhan (2008) who reported lower values of the von Kármán coefficient κ in APGs. Moreover, the APG TBLs also exhibit a more prominent wake than the ZPG, associated with stronger energetic structures in the outer region, as also observed by Monty *et al.* (2011). Monty *et al.* (2011) and Harun *et al.* (2013) showed that the APG energises the largest turbulent structures in the outer flow, leading to the more prominent wake, as well as to the outer peak in the streamwise velocity fluctuation profile. The most characteristic features of APG turbulent boundary layers in terms of the Reynolds-stress tensor components become apparent when compared to the ZPG case as shown in Figure 6(b,d) (Monty *et al.*, 2011): the streamwise velocity fluctuation profile develops an outer peak, a consequence of the energising of the large-scale motions, which also produces an increase of the near-wall peak due to the connection between the near-wall region and the outer flow. Note that the

location of this inner peak, $y^+ \simeq 15$, is essentially unaffected by the APG, and the amplitude of the inner peak appears to be approximately the same in the two cases. The wall-normal and spanwise velocity variance profiles, as well as the Reynolds shear-stress profile, exhibit a more prominent outer region compared to the ZPG due to the effect of the APG on the outer flow.

The previous comparison showed the great impact of the flow history in the state of a turbulent boundary layer, and in particular it highlighted the importance of constant- β cases as canonical representations of an APG TBL subjected to a certain pressure-gradient magnitude. In Figure 7 the inner-scaled mean velocity profile and selected components of the Reynolds-stress tensor for the cases with constant values of $\beta = 0, 1$ and 2 , i.e. the ZPG and two APG cases, are depicted for a matched value of $Re_\tau \simeq 700$. The interest of these configurations lies in the fact that they do not depend on flow history, and therefore can be considered as reference results for the corresponding β cases. Thus, the reported differences among cases are uniquely due to the pressure gradient, and not to flow history. The mean flow profile reveals the more prominent wake (connected to a lower skin-friction coefficient) at larger APGs, and also clearly shows the fact that the buffer layer lies below the one of the ZPG turbulent boundary layer, an effect that becomes more pronounced at progressively larger values of β . As opposed to what is observed in stronger APG conditions (Skåre and Krogstad, 1994), the cases under consideration in Figure 7 do not exhibit any differences in the viscous sublayer with respect to the ZPG. As discussed above, the APG also has an important effect in the Reynolds-stress tensor components, manifested in more energetic velocity fluctuation profiles, as well as Reynolds shear-stress profiles. This effect also becomes more pronounced for increasing values of β , and in the $\beta = 2$ case the magnitude of the outer peak in the streamwise velocity fluctuation profile is almost as large as that of the inner peak. An outer peak, which was not present in the ZPG case (but is expected to emerge at higher Re as discussed in Alfredsson *et al.*, 2011), also emerges in the other components of the

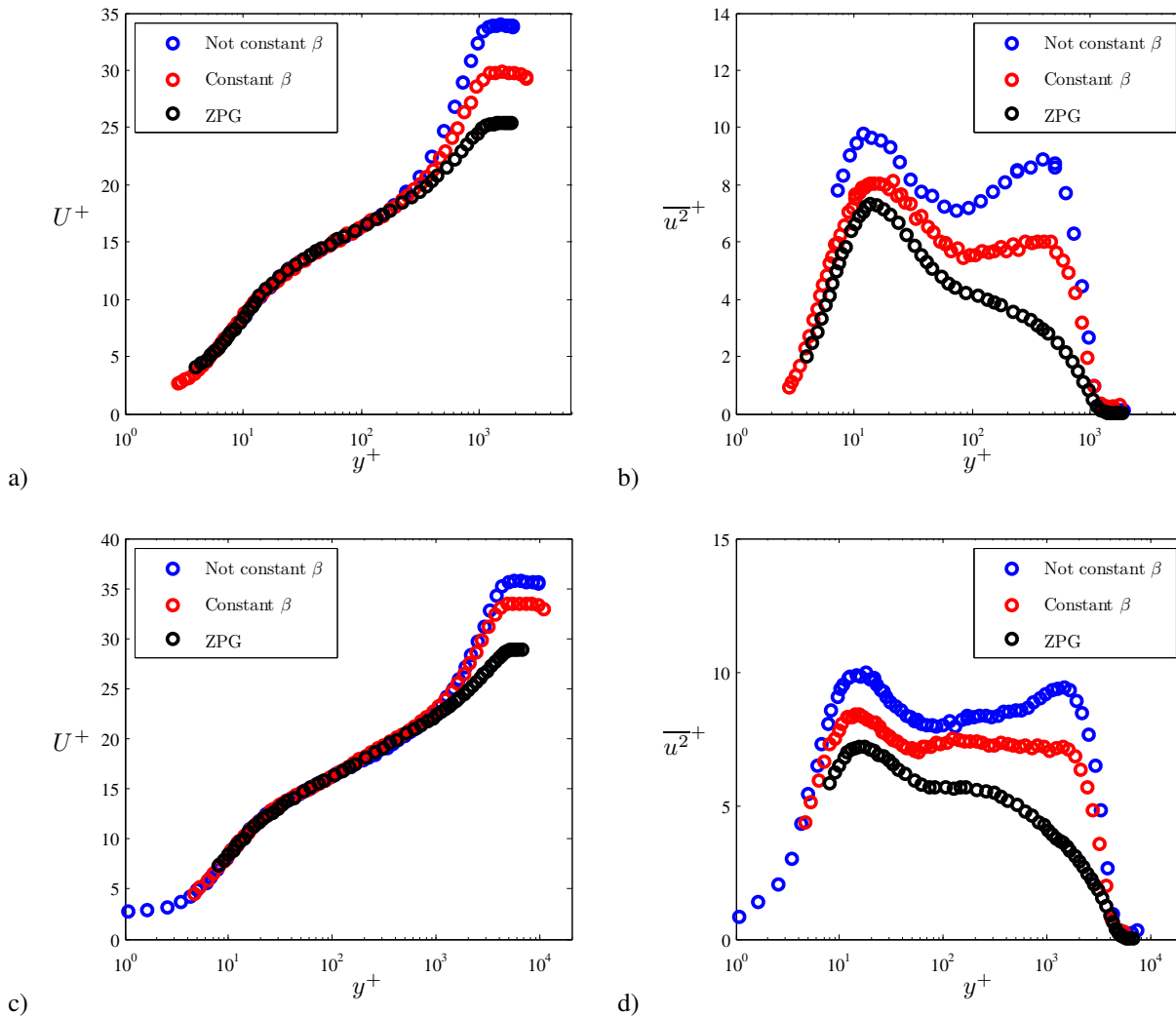


Figure 8. (a), (c) Inner-scaled profiles of the streamwise mean (b), (d) and variance, at case I and II from Figure 5b), i.e. $\beta \simeq 1.2$, $Re_\tau \simeq 1100$ and 4500 . ZPG TBL profile (Örlü and Schlatter, 2013) at matched Re_τ shown for comparison purposes.

Reynolds-stress tensor, the magnitude of which is proportional to the value of β . Another interesting observation from the Reynolds-stress profiles is the fact that, in the near-wall region, the streamwise and spanwise fluctuation profiles exhibit larger values for progressively stronger APG conditions.

To further extend the Reynolds-number range, Figure 8 shows profiles of the inner-scaled streamwise mean and variance from two cases with different history effects, but same $\beta \simeq 1.2$ and $Re_\tau \simeq 1100$ and 4500. Note that a ZPG turbulent boundary layer (i.e. $\beta = 0$) profile at matched Re_τ from Örlü and Schlatter (2013) is shown for comparison. As in the case from the lower Reynolds-number simulations, the results from the two APG cases from the wind-tunnel experiments also do not agree, although the local value of β is the same. The non-constant β case, which has been subjected to stronger APG conditions for a longer streamwise distance, exhibits a more prominent wake in the mean profile, as well as a stronger outer peak in the variance profile than the constant- β APG. It can therefore be stated that in order to assess the state of an APG TBL, it is necessary to consider not only the local pressure-gradient conditions, but also the streamwise evolution (or flow history) that led to that particular flow condition.

3. CONCLUSIONS

The present study is focused on the history effects in turbulent near-equilibrium boundary layers with adverse pressure gradients. After defining the near-equilibrium state according to Townsend (1976), large-eddy simulations were performed over a flat plate to assess the effect of different evolutions of the pressure-gradient parameter β . Hereby constant and non-constant pressure-gradient-parameter distributions were achieved and enabled the separation of Reynolds-number effects and pressure-gradient effects.

Ongoing accompanying studies have shown that APG TBLs with constant values of β can be described over a certain Re -range analogous to ZPG TBLs by means of a simple transformation (Vinueza *et al.*, 2017). Furthermore, the aforementioned comparison of components of the Reynolds-stress tensor, could also be extended to higher Reynolds numbers by means of the available PIV measurements (Sanmiguel Vila *et al.*, 2017a).

4. ACKNOWLEDGEMENTS

RÖ, RV and PS acknowledge the financial support from the Swedish Research Council (VR) and the Knut and Alice Wallenberg Foundation. The simulations were performed on resources provided by the Swedish National Infrastructure for Computing (SNIC) at the PDC Center for High Performance Computing at KTH Stockholm. RÖ acknowledges the financial support of the Lundequvist foundation. CSV acknowledges the financial support from Universidad Carlos III de Madrid within the program “Ayudas para la Movilidad del Programa Propio de Investigación”. CSV, SD and AI were partially supported by the COTURB project (Coherent Structures in Wall-bounded Turbulence), funded by the European Research Council (ERC), under grant ERC-2014.AdG-669505. AI, CSV and SD have been partially supported by grant DPI2016-79401-R of the Spanish Mincos.

5. REFERENCES

- Alfredsson, P.H. and Örlü, R., 2010. “The diagnostic plot—a litmus test for wall bounded turbulence data”. *Eur. J. Mech. B-Fluid*, Vol. 29, pp. 403–406.
- Alfredsson, P.H., Örlü, R. and Segalini, A., 2012. “A new formulation for the streamwise turbulence intensity distribution in wall-bounded turbulent flows”. *Eur. J. Mech. B-Fluid*, Vol. 36, pp. 167–175.
- Alfredsson, P.H., Segalini, A. and Örlü, R., 2011. “A new scaling for the streamwise turbulence intensity in wall-bounded turbulent flows and what it tells us about the “outer” peak”. *Phys. Fluids*, Vol. 23, p. 041702.
- Bobke, A., Vinueza, R. and Örlü, R., 2016. “Large-eddy simulations of adverse pressure gradient turbulent boundary layers”. *J. Phys.: Conf. Ser.*, Vol. 708, p. 012012.
- Bobke, A., Vinueza, R., Örlü, R. and Schlatter, P., 2017. “History effects and near-equilibrium in adverse-pressure-gradient turbulent boundary layers”. *J. Fluid Mech.*, (In Print).
- Chauhan, K.A., Monkewitz, P.A. and Nagib, H.M., 2009. “Criteria for assessing experiments in zero pressure gradient boundary layers”. *Fluid Dyn. Res.*, Vol. 41, No. 2, pp. 021404–24.
- Eitel-Amor, G., Örlü, R. and Schlatter, P., 2014. “Simulation and validation of a spatially evolving turbulent boundary layers up to $Re_\theta = 8300$ ”. *Int. J. Heat Fluid Flow*, Vol. 47, pp. 57–69.
- Eitel-Amor, G., Örlü, R., Schlatter, P. and Flores, O., 2015. “Hairpin vortices in turbulent boundary layers”. *Phys. Fluids*, Vol. 27, p. 025108.
- Fernholz, H.H. and Finley, P.J., 1996. “The incompressible zero-pressure-gradient turbulent boundary layer: An assessment of the data”. *Prog. Aerosp. Sci.*, Vol. 32, pp. 245–311.

- Harun, Z., Monty, J.P., Mathis, R. and Marusic, I., 2013. "Pressure gradient effects on the large-scale structure of turbulent boundary layers". *J. Fluid Mech.*, Vol. 715, pp. 477–498.
- Hosseini, S.M., Vinuesa, R., Schlatter, P., Hanifi, A. and Henningson, D.S., 2016. "Direct numerical simulation of the flow around a wing section at moderate Reynolds number". *Int. J. Heat Fluid Flow*, Vol. 61, pp. 117–128.
- Hoyas, S. and Jiménez, J., 2006. "Scaling of the velocity fluctuations in turbulent channels up to $Re_\tau=2003$ ". *Phys. Fluids*, Vol. 18, p. 011702.
- Lee, J.H. and Sung, H.J., 2008. "Effects of an adverse pressure gradient on a turbulent boundary layer". *Int. J. Heat Fluid Flow*, Vol. 29, pp. 568–578.
- Maciel, Y., Rossignol, K.S.P. and Lemay, J., 2006. "Self-similarity in the outer region of adverse-pressure-gradient turbulent boundary layers". *AIAA J.*, Vol. 44, pp. 2450–2464.
- Marusic, I., Mckeon, B.J., Monkewitz, P.A., Nagib, H.M., Smits, A.J. and Sreenivasan, K.R., 2010. "Wall-bounded turbulent flows at high Reynolds numbers: Recent advances and key issues". *Phys. Fluids*, Vol. 22, p. 065103.
- Mellor, G.L. and Gibson, D.M., 1966. "Equilibrium turbulent boundary layers". *J. Fluid Mech.*, Vol. 24, pp. 225–253.
- Monkewitz, P.A., Chauhan, K.A. and Nagib, H.M., 2008. "Comparison of mean flow similarity laws in zero pressure gradient turbulent boundary layers". *Phys. Fluids*, Vol. 20, p. 105102.
- Monty, J.P., Harun, Z. and Marusic, I., 2011. "A parametric study of adverse pressure gradient turbulent boundary layers". *Int. J. Heat Fluid Flow*, Vol. 32, pp. 575–585.
- Nagib, H.M. and Chauhan, K.A., 2008. "Variations of von Kármán coefficient in canonical flows". *Phys. Fluids*, Vol. 20, p. 101518.
- Nagib, H.M., Chauhan, K.A. and Monkewitz, P.A., 2007. "Approach to an asymptotic state for zero pressure gradient turbulent boundary layers". *Phil. Trans. R. Soc. A.*, Vol. 365, pp. 755–770.
- Örlü, R. and Alfredsson, P.H., 2010. "On spatial resolution issues related to time-averaged quantities using hot-wire anemometry". *Exp. Fluids*, Vol. 49, pp. 101–110.
- Örlü, R. and Schlatter, P., 2013. "Comparison of experiments and simulations for zero pressure gradient turbulent boundary layers at moderate Reynolds numbers". *Exp. Fluids*, Vol. 54, p. 1547.
- Örlü, R., Segalini, A., Klewicki, J. and Alfredsson, P.H., 2016. "High-order generalisation of the diagnostic scaling for turbulent boundary layers". *J. Turbulence*, Vol. 17, pp. 664–677.
- Patel, V.C. and Sotiropoulos, F., 1997. "Longitudinal curvature effects in turbulent boundary layers". *Prog. Aerosp. Sci.*, Vol. 33, pp. 1–70.
- Sanmiguel Vila, C., Örlü, R., Vinuesa, R., Schlatter, P., Ianiro, A. and Discetti, S., 2017a. "Adverse-pressure-gradient effects on turbulent boundary layers: a PIV study". *Flow Turbul. Combust.*, (submitted).
- Sanmiguel Vila, C., Vinuesa, R., Discetti, S., Ianiro, A., Schlatter, P. and Örlü, R., 2017b. "On the identification of well-behaved turbulent boundary layers". *J. Fluid Mech.*, (In Print).
- Schlatter, P., Li, Q., Brethouwer, G., Johansson, A.V. and Henningson, D.S., 2010. "Simulations of spatially evolving turbulent boundary layers up to $Re_\theta=4300$ ". *Int. J. Heat Fluid Flow*, Vol. 31, pp. 251–261.
- Schlatter, P., Li, Q., Örlü, R., Hussain, F. and Henningson, D.S., 2014. "On the near-wall vortical structures at moderate Reynolds numbers". *Eur. J. Mech. B-Fluid*, Vol. 48, pp. 75–93.
- Schlatter, P. and Örlü, R., 2010a. "Assessment of direct numerical simulation data of turbulent boundary layers". *J. Fluid Mech.*, Vol. 659, pp. 116–126.
- Schlatter, P. and Örlü, R., 2010b. "Quantifying the interaction between large and small scales in wall-bounded turbulent flows: A note of caution". *Phys. Fluids*, Vol. 22, No. 5, p. 051704.
- Schlatter, P. and Örlü, R., 2012. "Turbulent boundary layers at moderate Reynolds numbers: inflow length and tripping effects". *J. Fluid Mech.*, Vol. 710, pp. 5–34.
- Schlatter, P., Örlü, R., Li, Q., Brethouwer, G., Fransson, J.H.M., Johansson, A.V., Alfredsson, P.H. and Henningson, D.S., 2009. "Turbulent boundary layers up to $Re_\theta=2500$ studied through simulation and experiment". *Phys. Fluids*, Vol. 21, p. 051702.
- Skåre, P.E. and Krogstad, P.Å., 1994. "A turbulent equilibrium boundary layer near separation". *J. Fluid Mech.*, Vol. 272, pp. 319–348.
- Smits, A.J., Matheson, N. and Joubert, P.N., 1983. "Low-Reynolds-number turbulent boundary layers in zero and favorable pressure gradients". *J. Ship Res.*, Vol. 27, pp. 147–157.
- Townsend, A.A., 1976. "The structure of turbulent shear flow". *Cambridge University Press*, 2nd ed.
- Vinuesa, R., Bobke, A., Örlü, R. and Schlatter, P., 2016. "On determining characteristic length scales in pressure-gradient turbulent boundary layers". *Phys. Fluids*, Vol. 28, p. 055101.
- Vinuesa, R. and Örlü, R., 2017. "Measurement of wall shear stress." In: *Experimental Aerodynamics (Editors: Discetti, S. and Ianiro, A.)*, CRC Press Taylor & Francis Group.
- Vinuesa, R., Örlü, R., Sanmiguel Vila, C., Ianiro, A., Discetti, S. and Schlatter, P., 2017. "Revisiting history effects in adverse-pressure-gradient turbulent boundary layers". *Flow Turbul. Combust.*, (submitted).